Unified description of neutron superfluidity in the neutron-star crust with analogy to anisotropic multiband BCS superconductors

N. Chamel,[1,*] S. Goriely,[1] J. M. Pearson,[2] and M. Onsi[2]
[1]*Institut d'Astronomie et d'Astrophysique, CP-226, Université Libre de Bruxelles, 1050 Brussels, Belgium*
[2]*Département de Physique, Université de Montréal, Montréal, H3C 3J7 Québec, Canada*
(Received 10 March 2009; revised manuscript received 13 January 2010; published 13 April 2010)

The neutron superfluidity in the inner crust of a neutron star has traditionally been studied considering either homogeneous neutron matter or a small number of nucleons confined inside the spherical Wigner-Seitz cell. Drawing analogies with the recently discovered multiband superconductors, we have solved the anisotropic multiband BCS gap equations with Bloch boundary conditions, thus providing a unified description taking consistently into account both the free neutrons and the nuclear clusters. Calculations have been carried out using the effective interaction underlying our recent Hartree-Fock-Bogoliubov nuclear mass model HFB-16. We have found that even though the presence of inhomogeneities lowers the neutron pairing gaps, the reduction is much less than that predicted by previous calculations using the Wigner-Seitz approximation. We have studied the disappearance of superfluidity with increasing temperature. As an application we have calculated the neutron specific heat, which is an important ingredient for modeling the thermal evolution of newly born neutron stars. This work provides a new scheme for realistic calculations of superfluidity in neutron-star crusts.

DOI: 10.1103/PhysRevC.81.045804 PACS number(s): 26.60.Gj, 21.60.Jz, 97.60.Jd, 74.20.Fg

I. INTRODUCTION

The possibility of superfluidity inside neutron stars was suggested a long time ago by Migdal [1], only 2 years after the formulation of the theory of electron superconductivity by Bardeen, Cooper, and Schrieffer (BCS) [2] and before the discovery of the first pulsars. This prediction was later supported by the observation of the long relaxation time, of the order of months, following the first observed glitch in the Vela pulsar [3]. Glitches were subsequently observed in other pulsars. Pulsar glitches are believed to be related to the dynamics of the neutron superfluid permeating the inner layers of the solid neutron-star crust [4–6]. Understanding the properties of this neutron superfluid is also of prime importance for modeling the cooling of newly born neutron stars [7–10] and strongly magnetized neutron stars [11], the thermal relaxation of quasipersistent X-ray transients [12,13], or the quasiperiodic oscillations recently detected in the giant flares of Soft-Gamma Repeaters [14–16].

So far most microscopic studies of neutron superfluidity have been devoted to the case of uniform infinite neutron matter [17]. However, the coherence length of the neutron superfluid in the neutron-star crust is typically smaller than the lattice spacing and may even be comparable to the size of the nuclear clusters in some layers [18,19] (see also Sec. 8.2.3 of Ref. [20]). This situation is in sharp contrast to that encountered in ordinary type I electron superconductors, for which the electron Cooper pairs are spatially extended over macroscopic distances so that the order parameter is essentially uniform [21] (note that neutron stars are much too hot for electrons to be superconducting there; see, e.g., the discussion in Sec. 8.1 of Ref. [20]). The effects of the inhomogeneities on neutron superfluidity in the neutron-star crust have been studied in the mean-field approximation with realistic nucleon-nucleon potentials [22] and effective nucleon-nucleon interactions [9,10,23–26]. Systematic, fully self-consistent calculations in the entire inner crust (at zero temperature) have been recently carried out using semimicroscopic energy functionals [27]. In the latter work, it was found that even though inhomogeneities are small in the densest regions of the crust, the $^1S_0$ neutron pairing gaps are strongly reduced compared to those in uniform neutron matter. Moreover, the weaker the pairing force, the stronger is the suppression of the gaps. In somes cases, the gaps even vanish almost completely. All these quantum calculations have been carried out in the Wigner-Seitz (W-S) approximation, according to which the lattice is decomposed into a set of identical spherical cells centered around each cluster. The radius of each sphere is chosen so that its volume is equal to $1/\rho_N$, where ρ_N is the cluster density (number of lattice sites per unit volume). As discussed in Ref. [28], two different boundary conditions, yielding an almost-constant neutron density $\rho_n(\boldsymbol{r})$ near the cell edge, can be chosen. While the differences in the predicted pairing gaps are small for average nucleon densities, $\bar{\rho} \lesssim 0.03$ fm^{-3}, the uncertainties become increasingly large in the deeper layers of the crust [27]. This limitation of the W-S method is related to the existence of spurious neutron shell effects owing to the discretization of the single-particle (s.p.) energy spectrum [28,29].

In this paper, we present the first calculations of neutron superfluidity in neutron-star crusts going beyond the W-S approach by using the BCS theory of anisotropic multiband superconductivity. This theory is briefly reviewed in Sec. II. Our model of the neutron-star crust is discussed in Sec. III. The solutions of the BCS equations are presented in Sec. IV. We have focused on the deepest regions of the crust, for average nucleon densities $\bar{\rho}$ between 0.05 and 0.07 fm^{-3}, where the results from the W-S approximation are the most uncertain [27]. In Sec. V, we discuss the validity of the local density approximation (LDA) and the importance of proximity

*nchamel@ulb.ac.be

effects. The disappearance of superfluidity with increasing temperature is studied in Secs. VI and VII. In Sec. VIII, we present numerical results of the neutron specific heat.

II. BCS THEORY OF SUPERFLUID NEUTRONS IN NEUTRON-STAR CRUSTS

The standard formulation of the BCS theory starts with the Hamiltonian [2]

$$H = \sum_{\sigma,\alpha,\boldsymbol{k}} (\varepsilon_{\alpha\boldsymbol{k}} - \mu) c^{\dagger}_{\alpha\boldsymbol{k}\sigma} c_{\alpha\boldsymbol{k}\sigma} + \sum_{\alpha,\beta,\boldsymbol{k},\boldsymbol{k}'} V_{\alpha\boldsymbol{k}\beta\boldsymbol{k}'} c^{\dagger}_{\alpha\boldsymbol{k}\uparrow} c^{\dagger}_{\alpha-\boldsymbol{k}\downarrow} c_{\beta-\boldsymbol{k}'\downarrow} c_{\beta\boldsymbol{k}'\uparrow}, \quad (1)$$

where $c^{\dagger}_{\alpha\boldsymbol{k}\sigma}$ ($c_{\alpha\boldsymbol{k}\sigma}$) are the creation (annihilation) operators for Bloch states with wave vector $\boldsymbol{k}$, band index α, and spin σ, $\varepsilon_{\alpha\boldsymbol{k}}$ are the s.p. energies (assumed to be independent of the spin state), μ is chemical potential, and $V_{\alpha\boldsymbol{k}\beta\boldsymbol{k}'}$ are the matrix elements of the two-body pairing interaction. In the mean-field approximation at finite temperature, the quasiparticle (q.p.) energies are given by

$$E_{\alpha\boldsymbol{k}} = \sqrt{(\varepsilon_{\alpha\boldsymbol{k}} - \mu)^2 + \Delta^2_{\alpha\boldsymbol{k}}}, \quad (2)$$

where $\Delta_{\alpha\boldsymbol{k}}$ are solutions of the anisotropic multiband BCS gap equations (setting the Boltzmann constant $k_{\mathrm{B}} = 1$):

$$\Delta_{\alpha\boldsymbol{k}} = -\frac{1}{2} \sum_{\beta} \sum_{\boldsymbol{k}'} V_{\alpha\boldsymbol{k}\beta\boldsymbol{k}'} \frac{\Delta_{\beta\boldsymbol{k}'}}{E_{\beta\boldsymbol{k}'}} \tanh \frac{E_{\beta\boldsymbol{k}'}}{2T}. \quad (3)$$

In conventional superconductors the pairing interaction is induced by electron-phonon coupling [21]. It is usually a very good approximation to take the matrix elements $V_{\alpha\boldsymbol{k}\beta\boldsymbol{k}'}$ as constant and nonzero only within a low-energy shell, of the order $\sim \hbar\omega_{\mathrm{p}}$ around the Fermi level, where ω_{p} is the ion-plasma frequency. In this case the gap parameters $\Delta_{\alpha\boldsymbol{k}}$ depend neither on the band index α nor on the wave vector $\boldsymbol{k}$ and are all equal to a single constant, the pairing gap Δ [2]. The possibility of multiband superconductors characterized by the existence of several pairing gaps Δ_α was raised soon after the formulation of the BCS theory [30], but clear experimental evidence was lacking until the discovery in 2001 of superconductivity in magnesium diboride, whose unusual properties can be nicely explained by a two-band model [31,32]. Since then, many other multiband superconductors have been found such as the iron pnictide superconductors [33]. In these materials, several bands can intersect the Fermi level, yielding a complex, multisheeted Fermi surface. Pairing is still thought to be mediated by the exchange of phonons, but the electrons on the different sheets of the Fermi surface undergo very different pairing interactions, leading to the existence of different gaps. In the neutron-star crust, the formation of neutron pairs giving rise to superfluidity is directly triggered by the strong neutron-neutron interaction that is always attractive at low densities in the $^1S_0$ channel. The number of bands contributing appreciably to the pairing gap $\Delta_{\alpha\boldsymbol{k}}$ can thus be huge (about 10^2–10^3 in the dense layers of the inner crust considered in this work). Because the matrix elements of the pairing force may *a priori* vary appreciably, we have solved Eqs. (3) in the most general case.

III. MODEL OF THE NEUTRON-STAR CRUST

We have determined the equilibrium structure and composition of the inner crust of neutron stars by using the fourth-order Extended Thomas-Fermi method with quantum shell effects added via the Strutinsky-Integral theorem. This so-called ETFSI method, as applied to the equation of state of neutron-star crusts, has been described in detail in Ref. [34]. It is a high-speed approximation to the self-consistent Hartree-Fock method. We have neglected the small neutron shell effects [35], the estimation of which,in current calculations, is plagued by the approximate treatment of the interaction between the unbound neutrons and the nuclear lattice [28,29]. The calculations have been carried out using an effective nucleon-nucleon interaction of the Skyrme type:

$$\begin{aligned} v^{\mathrm{Sky}}(\boldsymbol{r}_i, \boldsymbol{r}_j) = {} & t_0(1 + x_0 P_\sigma)\delta(\boldsymbol{r}_{ij}) \\ & + \frac{1}{2} t_1 (1 + x_1 P_\sigma) \frac{1}{\hbar^2} \left[\boldsymbol{p}^2_{ij} \delta(\boldsymbol{r}_{ij}) + \delta(\boldsymbol{r}_{ij}) \boldsymbol{p}^2_{ij} \right] \\ & + t_2 (1 + x_2 P_\sigma) \frac{1}{\hbar^2} \boldsymbol{p}_{ij} \cdot \delta(\boldsymbol{r}_{ij}) \boldsymbol{p}_{ij} \\ & + \frac{1}{6} t_3 (1 + x_3 P_\sigma) \rho(\boldsymbol{r})^\gamma \delta(\boldsymbol{r}_{ij}) \\ & + \frac{\mathrm{i}}{\hbar^2} W_0 (\boldsymbol{\sigma}_i + \boldsymbol{\sigma}_j) \cdot \boldsymbol{p}_{ij} \times \delta(\boldsymbol{r}_{ij}) \boldsymbol{p}_{ij}, \end{aligned} \quad (4)$$

where $\boldsymbol{r}_{ij} = \boldsymbol{r}_i - \boldsymbol{r}_j$, $\boldsymbol{r} = (\boldsymbol{r}_i + \boldsymbol{r}_j)/2$, $\boldsymbol{p}_{ij} = -\mathrm{i}\hbar(\nabla_i - \nabla_j)/2$ is the relative momentum, P_σ is the two-body spin-exchange operator, and $\rho(\boldsymbol{r})$ is the total nucleon density at position $\boldsymbol{r}$. The pairing interaction that we take here acts only between nucleons of the same charge state q ($q = n$ or p for neutron or proton, respectively) and is given by

$$v^{\mathrm{pair}}_q(\boldsymbol{r}_i, \boldsymbol{r}_j) = v^{\pi q}[\rho_n(\boldsymbol{r}), \rho_p(\boldsymbol{r})] \delta(\boldsymbol{r}_{ij}), \quad (5)$$

where $\boldsymbol{r}_{ij} = \boldsymbol{r}_i - \boldsymbol{r}_j$, $\boldsymbol{r} = (\boldsymbol{r}_i + \boldsymbol{r}_j)/2$ and $\rho_n(\boldsymbol{r})$ and $\rho_p(\boldsymbol{r})$ are the neutron and proton density at position $\boldsymbol{r}$, respectively.

We have adopted the parametrization BSk16, underlying the HFB-16 nuclear mass model [36]. The parameters of this force are listed in Table I. This force is particularly suitable for studying neutron-rich environments such as neutron-star crusts, as it has been constrained to reproduce the equation of state and the $^1S_0$ pairing gap of infinite homogeneous neutron matter, as calculated for the realistic Argonne v_{14} potential and shown in Fig. 1. The expression of $v^{\pi q}[\rho_n(\boldsymbol{r}), \rho_p(\boldsymbol{r})]$ is given in Ref. [36]. Moreover, we can hope that the nuclear inhomogeneities in the neutron-star crust will be properly taken into account, given the excellent fit to essentially all the available experimental nuclear mass data.

To solve the BCS Eqs. (3), we first need to determine the neutron s.p. energies $\varepsilon_{\alpha\boldsymbol{k}}$ and wave functions $\varphi_{\alpha\boldsymbol{k}}(\boldsymbol{r})$. For this purpose, we have solved the following three-dimensional Schroedinger equation:

$$-\nabla \cdot \frac{\hbar^2}{2M^*_n(\boldsymbol{r})} \nabla \varphi_{\alpha\boldsymbol{k}}(\boldsymbol{r}) + U_n(\boldsymbol{r}) \varphi_{\alpha\boldsymbol{k}}(\boldsymbol{r}) = \varepsilon_{\alpha\boldsymbol{k}} \varphi_{\alpha\boldsymbol{k}}(\boldsymbol{r}). \quad (6)$$

The effective mass $M^*_n(\boldsymbol{r})$ and the potential $U_n(\boldsymbol{r})$ are given by (we neglect the small rearrangement term coming from the

TABLE I. Skyrme parameters of the force BSk16 [36]. ε_Λ is a s.p. energy cutoff above the chemical potential introduced to regularize the divergences associated with the zero range of the pairing force.

t_0 (MeV fm^3)	−1837.23
t_1 (MeV fm^5)	383.521
t_2 (MeV fm^5)	−3.41736
t_3 (MeV fm$^{3+3\gamma}$)	11523.0
x_0	0.432600
x_1	−0.824106
x_2	44.6520
x_3	0.689797
W_0 (MeV fm^5)	141.100
γ	0.3
ε_Λ (MeV)	16

pairing force; see, e.g., Ref. [36])

$$\frac{\hbar^2}{2M_n^*} = \frac{\hbar^2}{2M_n} + \frac{1}{4}t_1\left[\left(1+\frac{1}{2}x_1\right)\rho - \left(\frac{1}{2}+x_1\right)\rho_n\right] + \frac{1}{4}t_2\left[\left(1+\frac{1}{2}x_2\right)\rho + \left(\frac{1}{2}+x_2\right)\rho_n\right], \tag{7}$$

$$\begin{aligned} U_n = {} & t_0\left[\left(1+\tfrac{1}{2}x_0\right)\rho - \left(\tfrac{1}{2}+x_0\right)\rho_n\right] + \tfrac{1}{4}t_1\left[\left(1+\tfrac{1}{2}x_1\right)\right. \\ & \times\left(\tau - \tfrac{3}{2}\nabla^2\rho\right) - \left(\tfrac{1}{2}+x_1\right)\left(\tau_n - \tfrac{3}{2}\nabla^2\rho_n\right)\left.\right] \\ & + \tfrac{1}{4}t_2\left[\left(1+\tfrac{1}{2}x_2\right)\left(\tau + \tfrac{1}{2}\nabla^2\rho\right) + \left(\tfrac{1}{2}+x_2\right)\right. \\ & \times\left(\tau_n + \tfrac{1}{2}\nabla^2\rho_n\right)\left.\right] + \tfrac{1}{12}t_3\left[\left(1+\tfrac{1}{2}x_3\right)(2+\gamma)\rho^{\gamma+1}\right. \\ & \left. - \left(\tfrac{1}{2}+x_3\right)\left(2\rho^\gamma\rho_n + \gamma\rho^{\gamma-1}\left(\rho_n^2+\rho_p^2\right)\right)\right], \end{aligned} \tag{8}$$

where $\tau_n(\boldsymbol{r})$ and $\tau_p(\boldsymbol{r})$ are the neutron and proton kinetic-energy densities, respectively (we have introduced $\tau = \tau_n + \tau_p$). Both $M_n^*(\boldsymbol{r})$ and $U_n(\boldsymbol{r})$ were determined using the ETFSI fields. In Eq. (6), we have neglected the spin-orbit coupling arising from the last term in Eq. (4). This approximation is justified because the spin-orbit coupling is proportional to $\nabla\rho_n$ and $\nabla\rho_p$ (see, e.g., Appendix A of Ref. [36]). In the neutron-star crust, nuclear clusters have a very diffuse surface, as shown in Fig. 2, and consequently the spin-orbit coupling is much smaller than that in isolated nuclei [29].

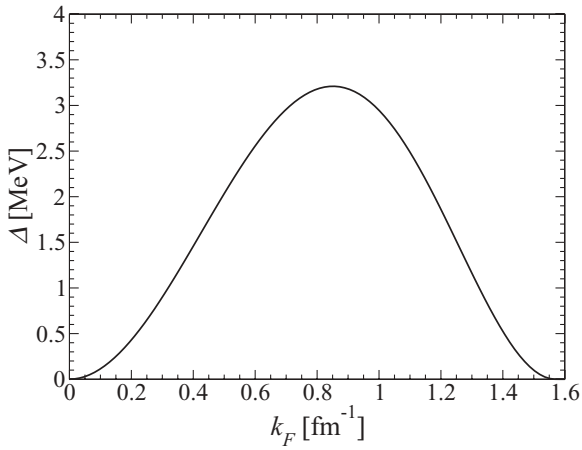

FIG. 1. $^1S_0$ neutron pairing gap in infinite uniform neutron matter versus Fermi wave number $k_F = (3\pi^2\rho_n)^{1/3}$, as used in model HFB-16 [36].

Although neutron shell effects represent a small correction to the total energy density [35], they are expected to have a much stronger impact on neutron superfluidity owing to the highly nonlinear nature of the pairing phenomenon. This is the reason why we have not followed the usual practice of applying the W-S approximation for solving Eq. (6), but have imposed the Bloch boundary conditions,

$$\varphi_{\alpha\boldsymbol{k}}(\boldsymbol{r}+\boldsymbol{\ell}) = \exp(\mathrm{i}\boldsymbol{k}\cdot\boldsymbol{\ell})\varphi_{\alpha\boldsymbol{k}}(\boldsymbol{r}), \tag{9}$$

where $\boldsymbol{\ell}$ denotes any lattice translation vector. Note that, in this case, Eq. (6) has to be solved for each wave vector $\boldsymbol{k}$, while in the W-S method only a single wave vector is considered, namely, $\boldsymbol{k} = 0$ (see Ref. [29] for a discussion about the W-S approximation). Following the standard assumptions, we have considered a body-centered cubic lattice [20]. The BCS Hamiltonian (1) can then be obtained from the s.p. states, once the pairing interaction has been specified. The matrix elements of the pairing force (5) between Bloch states are given by an integral over the W-S cell of volume $\mathcal{V}_{\rm cell}$,

$$V_{\alpha\boldsymbol{k}\beta\boldsymbol{k}'} = \int_{\rm WS} \mathrm{d}^3r\, v^\pi[\rho_n(\boldsymbol{r})]|\varphi_{\alpha\boldsymbol{k}}(\boldsymbol{r})|^2|\varphi_{\beta\boldsymbol{k}'}(\boldsymbol{r})|^2, \tag{10}$$

the Bloch wave functions $\varphi_{\alpha\boldsymbol{k}}(\boldsymbol{r})$ being normalized according to

$$\int_{\rm WS} \mathrm{d}^3r|\varphi_{\alpha\boldsymbol{k}}(\boldsymbol{r})|^2 = 1. \tag{11}$$

The W-S cell that we consider here is a truncated octahedron, as determined by the body-centered cubic lattice geometry. It should not be confused with the spherical cell used in the W-S approximation [29].

IV. NEUTRON PAIRING GAPS

We have considered five different layers of the inner crust in the average nucleon density range between 0.05 and 0.07 fm^{-3}. Results of the ETFSI calculations at $T = 0$ are summarized in Table II and the nucleon density profiles are plotted in Fig. 2.

We have solved iteratively the anisotropic multiband BCS gap equations (3) for each average nucleon density $\bar\rho$. Results

TABLE II. Ground-state composition of the neutron-star crust using the ETFSI method with Skyrme force BSk16. $\bar\rho$ is the average nucleon density, Z and A are the equilibrium numbers of protons and nucleons in the W-S cell, respectively, and ρ_{Bn} is the neutron background density outside clusters (see Ref. [34]).

$\bar\rho$ (fm^{-3})	Z	A	ρ_{Bn} (fm^{-3})
0.070	40	1258	0.060
0.065	40	1264	0.056
0.060	40	1260	0.051
0.055	40	1294	0.047
0.050	40	1304	0.043

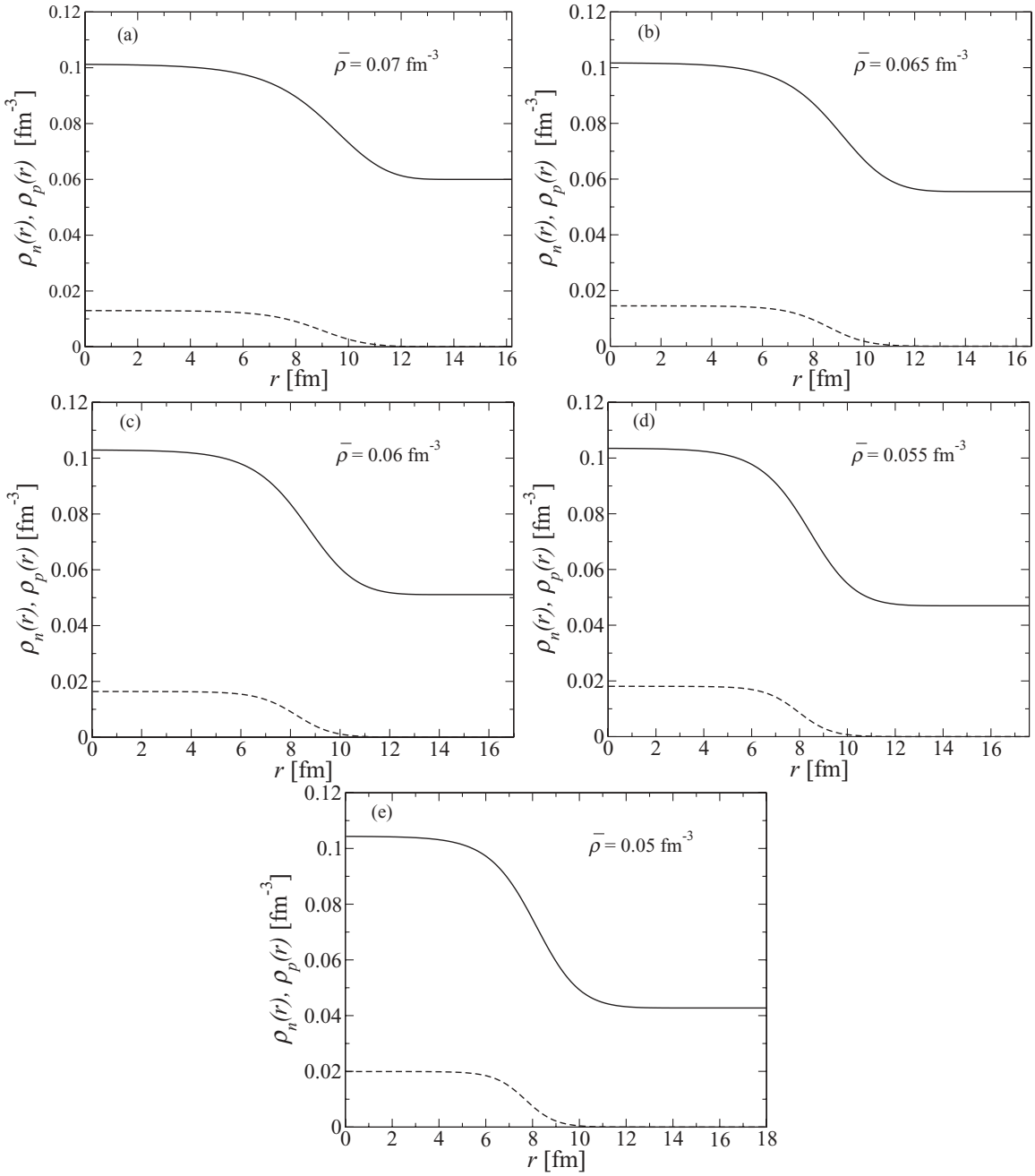

FIG. 2. Equilibrium neutron number density $\rho_n(r)$ (solid line) and proton number density $\rho_p(r)$ (dashed line) inside the Wigner-Seitz cell of different neutron-star crust layers with average nucleon density $\bar{\rho}$. The densities (in fm^{-3}) were obtained using the ETFSI method [34] at $T = 0$ with the Skyrme force BSk16 [36].

are summarized in Table III. Owing to the ultraviolet divergence induced by the zero range of the pairing interaction (5), the summation in Eq. (3) has to be truncated. We have imposed the same s.p. energy cutoff, $\varepsilon_\Lambda = 16$ MeV, above the chemical potential as used in the determination of the BSk16 force through optimization of the mass fit. For each temperature the chemical potential has been recalculated neglecting pairing, as the pairing gaps are much smaller than the Fermi energy (note that the same approximation was used in Ref. [36] to construct the effective density-dependent pairing strength from the pairing gap in infinite homogeneous neutron matter). We have solved Eq. (6) by expanding the s.p. wave functions into plane waves,

$$\varphi_{\alpha\boldsymbol{k}}(\boldsymbol{r}) = \exp(\mathrm{i}\boldsymbol{k}\cdot\boldsymbol{r}) \sum_{\boldsymbol{G}} \widetilde{\varphi}_{\alpha\boldsymbol{k}}(\boldsymbol{G}) \exp(\mathrm{i}\boldsymbol{G}\cdot\boldsymbol{r}), \tag{12}$$

in which $\boldsymbol{G}$ are reciprocal lattice vectors. Because by definition

$$\exp(\mathrm{i}\boldsymbol{G}\cdot\boldsymbol{\ell}) = 1 \tag{13}$$

for any vectors $\boldsymbol{G}$ and $\boldsymbol{\ell}$, the Bloch boundary conditions (9) are automatically satisfied. We have included all Fourier components with reciprocal lattice vectors $\boldsymbol{G}$ such that $|\boldsymbol{k} + \boldsymbol{G}| < Q$.

TABLE III. Neutron pairing gaps in the neutron-star crust for different average nucleon densities $\bar{\rho}$ at $T = 0$. Δ_F (Δ_{F0}) is the pairing gap obtained from Eq. (3) after averaging over continuum states and using the special point method (mean-value point method) for the summation over $\boldsymbol{k}$. Δ_u and $\bar{\Delta}_u$ are the pairing gaps in uniform infinite neutron matter for the neutron density ρ_{Bn} and for the average neutron density $\bar{\rho}_n = (A - Z)/\mathcal{V}_{cell}$, respectively.

$\bar{\rho}$ (fm^{-3})	Δ_F (MeV)	Δ_{F0} (MeV)	Δ_u (MeV)	$\bar{\Delta}_u$ (MeV)
0.070	1.44	1.39	1.79	1.43
0.065	1.65	1.59	1.99	1.65
0.060	1.86	1.81	2.20	1.87
0.055	2.08	2.07	2.40	2.10
0.050	2.29	2.27	2.59	2.33

Q has been adjusted so that the s.p. energies are computed with an accuracy of a few keV. We have evaluated the summation in Eq. (3) using the special-point method [37]. We have also applied this method to compute the pairing matrix elements (10). On general grounds one may expect that $|\varphi_{\alpha\boldsymbol{k}}(\boldsymbol{r})|^2$, and thereby $V_{\alpha\boldsymbol{k}\beta\boldsymbol{k}'}$ and $\Delta_{\alpha\boldsymbol{k}}$, are weakly dependent on $\boldsymbol{k}$, because bound states are vanishingly small outside clusters where Bloch boundary conditions are imposed, while continuum states depend on $\boldsymbol{k}$ essentially through only a phase factor, $\exp(i\boldsymbol{k}\cdot\boldsymbol{r})$. Indeed we have found that the summation in Eq. (3) converges quickly with the number of special $\boldsymbol{k}$ points. An error below 1% for the averaged pairing gap Δ_F can be reached with 30 $\boldsymbol{k}$ points. Keeping just one term, corresponding to the mean-value point [38], yields a result with a few percent precision, as reported in Table III. This method has indeed proved to be surprisingly accurate in solid-state physics to compute the electron density and dielectric matrix [39]. The convergence of the real-space integrations in Eq. (10) is slower because of the oscillating behavior of the wave functions. We have checked that the solutions of the BCS gap equations converge to a few-keV accuracy using 110 special $\boldsymbol{r}$ points.

As shown in Fig. 3, the dependence of the pairing gaps $\Delta_{\alpha\boldsymbol{k}}$ on the band index α and wave vector $\boldsymbol{k}$ is quite significant. At the Fermi level the pairing gaps vary by about ∼0.2–0.4 MeV. While all s.p. states lying in the continuum contribute to the average gap Δ_F, we have found that Δ_F remains almost unchanged if bound states are excluded from the summation in Eq. (3). However, this does not imply that neutrons inside clusters do not have any impact on the average pairing gap. The inhomogeneous distribution of neutrons modifies the s.p. energies and the matrix elements of the pairing force.

For comparison, we have calculated the neutron pairing gap Δ_u without nuclear clusters, assuming that unbound neutrons are uniformly distributed, with the density ρ_{Bn} corresponding to the neutron background density outside clusters (values of ρ_{Bn} for the different crustal layers are indicated in Table II). In this limiting case, the Bloch wave functions reduce to plane waves,

$$\varphi_{\alpha\boldsymbol{k}}(\boldsymbol{r}) = \frac{1}{\sqrt{\mathcal{V}_{cell}}}\exp[i,(\boldsymbol{k}+\boldsymbol{G}_\alpha)\cdot\boldsymbol{r}], \tag{14}$$

where $\boldsymbol{G}_\alpha$ are reciprocal lattice vectors. The pairing matrix elements all become equal,

$$V_{\alpha\boldsymbol{k}\beta\boldsymbol{k}'} = \frac{v^\pi[\rho_{Bn}]}{\mathcal{V}_{cell}}. \tag{15}$$

As a result, the pairing gaps are independent of α and $\boldsymbol{k}$ and are the solutions of the usual isotropic BCS equations [2]:

$$1 = -\frac{v^\pi[\rho_{Bn}]}{8\pi^2}\left(\frac{2M^*_{Bn}}{\hbar^2}\right)^{3/2}\int_0^{\varepsilon_{BF}+\varepsilon_\Lambda} d\varepsilon\,\frac{\sqrt{\varepsilon}}{E(\varepsilon)}\tanh\frac{E(\varepsilon)}{2T}, \tag{16}$$

with

$$E(\varepsilon) = \sqrt{(\varepsilon-\varepsilon_{BF})^2+\Delta_u^2}, \tag{17}$$

in which

$$\varepsilon_{BF} = \frac{\hbar^2 k_{FB}^2}{2M^*_{Bn}} \tag{18}$$

is the Fermi energy, $k_{FB} = (3\pi^2\rho_{Bn})^{1/3}$, and M^*_{Bn} is the effective mass in neutron matter at density ρ_{Bn}. From the definition of the pairing strength, it follows immediately that Δ_u at $T = 0$ is nothing but the microscopic neutron pairing gap, shown in Fig. 1, evaluated at the neutron density $\rho_n = \rho_{Bn}$. Results for the different crust layers are reported in Table III. Comparing Δ_F and Δ_u, it can be seen that the presence of inhomogeneities lowers the averaged neutron pairing gap by about 10–20%. This reduction is much smaller than that found in previous calculations based on the W-S approach [27]. For instance, for $\bar{\rho} = 0.058$ fm^{-3}, Δ_F was suppressed by about 40–60%, depending on the choice of boundary conditions (last line in Table 2 in Ref. [27]).

V. PAIRING FIELD OF THE NEUTRON SUPERFLUID AT ZERO TEMPERATURE AND LOCAL DENSITY APPROXIMATION

The effects of the inhomogeneities on the neutron superfluid can be seen more directly by computing the neutron pairing field, defined by

$$\Delta_n(\boldsymbol{r}) = -\tfrac{1}{2}v^{\pi n}[\rho_n(\boldsymbol{r}),\rho_p(\boldsymbol{r})]\tilde{\rho}_n(\boldsymbol{r}), \tag{19}$$

where $\rho_n(\boldsymbol{r})$ and $\tilde{\rho}_n(\boldsymbol{r})$ are the local normal neutron density and abnormal neutron density, respectively, given (at $T = 0$) by

$$\rho_n(\boldsymbol{r}) = \sum_{\alpha,\boldsymbol{k}}^{\Lambda}|\varphi_{\alpha\boldsymbol{k}}(\boldsymbol{r})|^2\left[1-\frac{\varepsilon_{\alpha\boldsymbol{k}}-\mu}{E_{\alpha\boldsymbol{k}}}\right], \tag{20}$$

$$\tilde{\rho}_n(\boldsymbol{r}) = \sum_{\alpha,\boldsymbol{k}}^{\Lambda}|\varphi_{\alpha\boldsymbol{k}}(\boldsymbol{r})|^2\frac{\Delta_{\alpha\boldsymbol{k}}}{E_{\alpha\boldsymbol{k}}}, \tag{21}$$

where the superscript Λ is to indicate that the summation includes only states whose s.p. energy lies below $\mu+\varepsilon_\Lambda$. We have computed the angle-averaged pairing field inside each W-S cell, as given by

$$\Delta_n(\boldsymbol{r}) = \int_{WS}\frac{d\Omega}{4\pi}\Delta_n(\boldsymbol{r}). \tag{22}$$

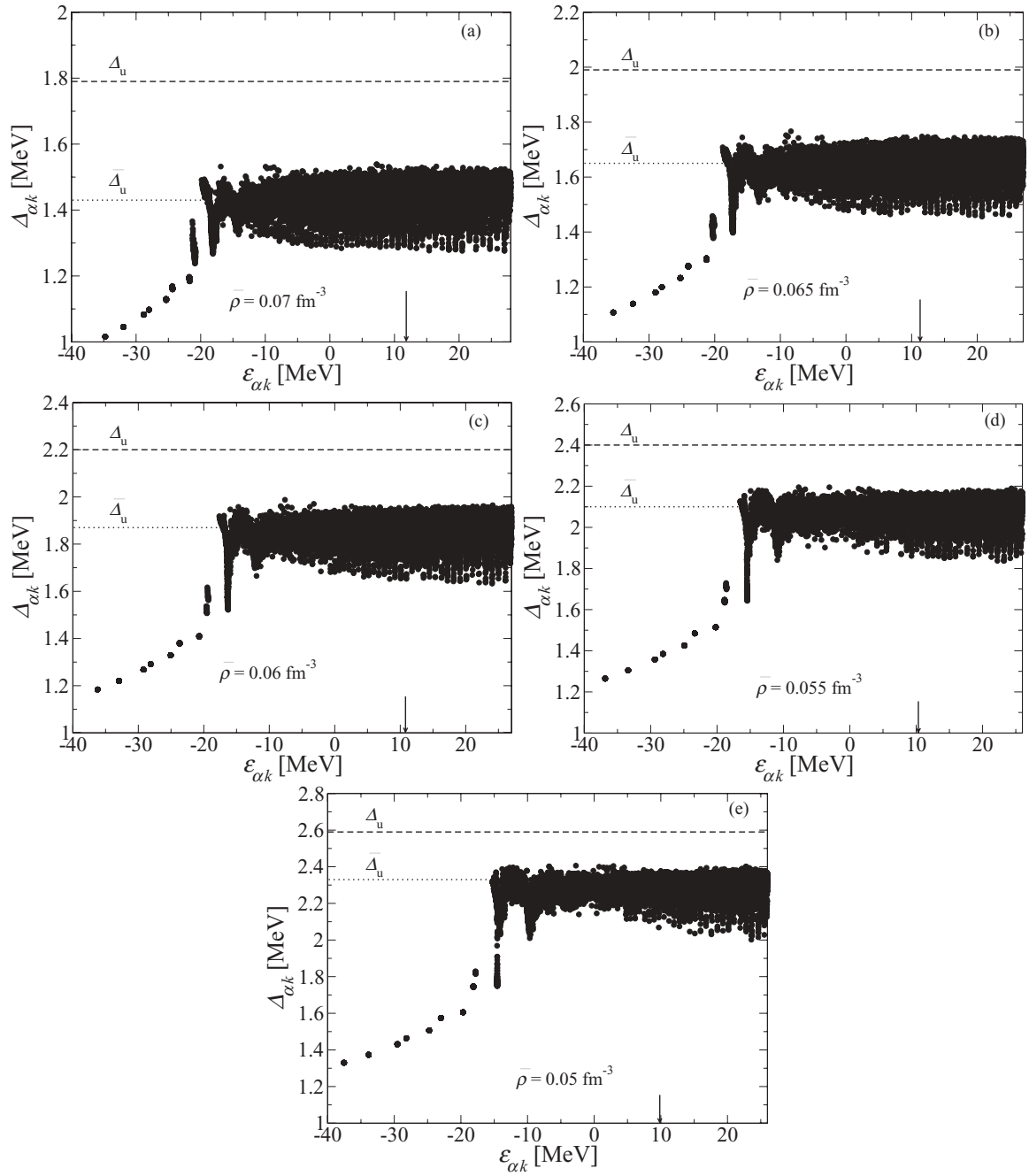

FIG. 3. Neutron pairing gaps $\Delta_{\alpha k}$ versus s.p. energies $\varepsilon_{\alpha k}$ for the different crustal layers. The arrow indicates the position of the chemical potential at $T = 0$. The BCS equations (3) have been solved at $T = 0$ together with Eq. (6) using the neutron-star crust composition shown in Fig. 2. The dashed and dotted horizontal lines represent the gaps Δ_u and $\bar{\Delta}_u$, respectively, given in Table III.

For each value of the radial coordinate r, we have performed the solid-angle integration using 30 uniformly distributed spiral points on the sphere of radius r [40]. To minimize the amount of computations, we have applied the mean-value point method for solving the BCS equations and for calculating the normal and abnormal densities. For comparison, we have also calculated the pairing field in the LDA, that is, assuming that at each point $\boldsymbol{r}$ the pairing field is locally the same as that in uniform neutron matter for the density $\rho_n(\boldsymbol{r})$:

$$\Delta_n^{(\mathrm{LDA})}(\boldsymbol{r}) = \Delta_u(\rho_n(\boldsymbol{r})). \tag{23}$$

As shown in Fig. 4, the LDA overestimates the spatial dependence of the pairing field, thus indicating that pairing is highly nonlocal. Indeed the local coherence length of the neutron superfluid, defined by [2]

$$\xi(\boldsymbol{r}) = \frac{\hbar^2 k_{\mathrm{F}}(\boldsymbol{r})}{\pi M_n^*(\boldsymbol{r}) \Delta_n^{(\mathrm{LDA})}(\boldsymbol{r})}, \tag{24}$$

where

$$k_{\mathrm{F}}(\boldsymbol{r}) = (3\pi^2 \rho_n(\boldsymbol{r}))^{1/3}, \tag{25}$$

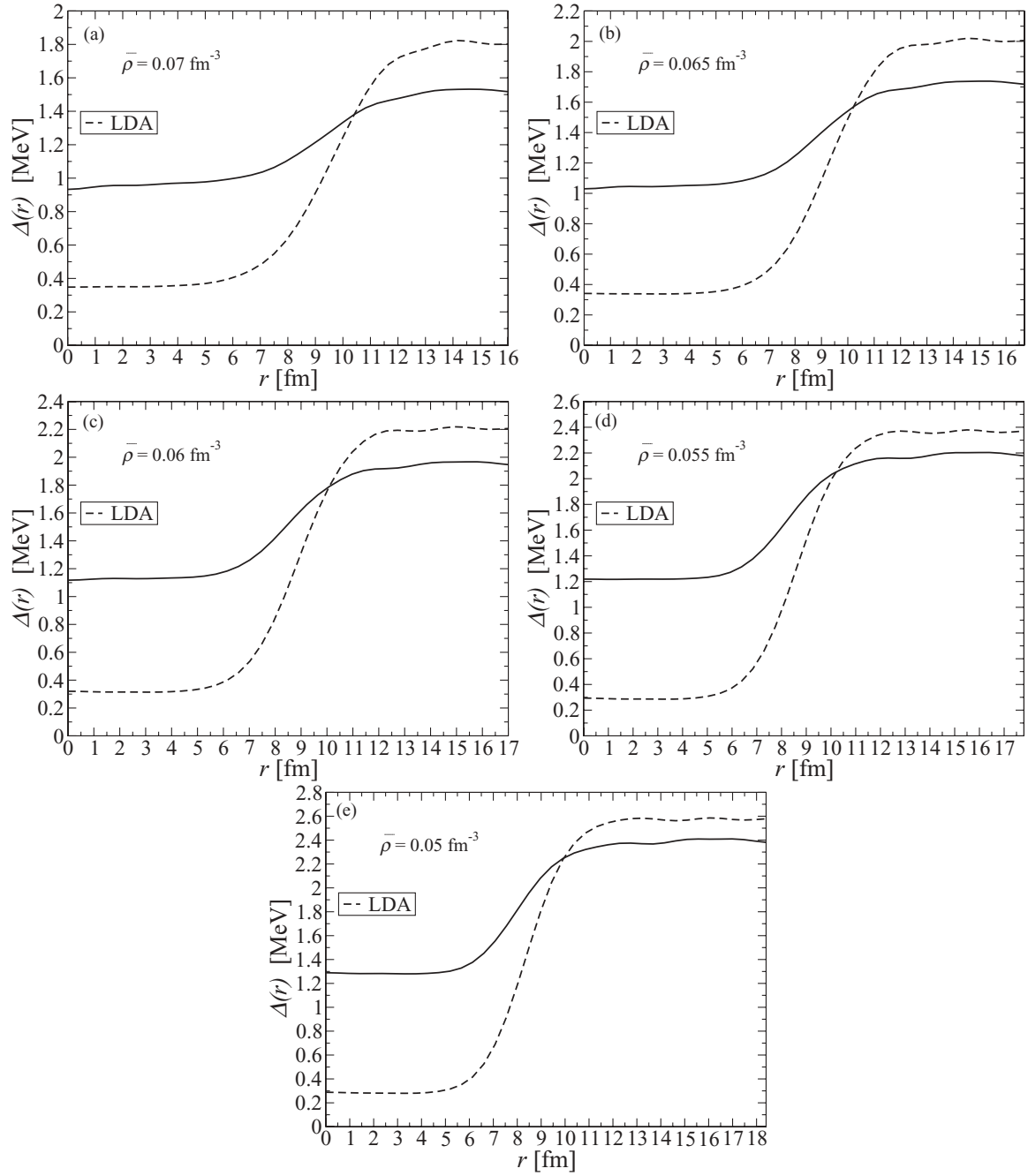

FIG. 4. Angle-averaged neutron pairing field $\Delta(r)$ (solid line) and LDA pairing field (dashed line) for the different crustal layers at $T = 0$.

is larger than the size of the clusters, as shown in Fig. 5. This means that even if the center of mass of a Cooper pair is located outside clusters, one of the partners may actually lie inside so that all neutrons are actually involved in the pairing process. As a result, pairing correlations are strongly enhanced inside clusters but are reduced in the intersticial region, leading to a smooth spatial variation of the pairing field. These so-called proximity effects are the most spectacular in the shallowest layer, at $\bar{\rho} = 0.05$ fm^{-3}, where the neutron pairing field is increased by a factor of $\sim$4 inside clusters. The entire inner crust is therefore permeated by the neutron superfluid, including in the region occupied by clusters themselves.

The previous considerations suggest estimating $\Delta_{\rm F}$ by calculating the pairing gap $\bar{\Delta}_{\rm u}$ in uniform neutron matter for the average neutron density $\bar{\rho}_n \equiv N/\mathcal{V}_{\rm cell}$ instead of the neutron background density ρ_{Bn}. As reported in Table III, this gap indeed provides a very good approximation of the average gap calculated numerically.

VI. CRITICAL TEMPERATURE

While the pairing gaps obtained from Eqs. (3) vary from one band to the other as shown in Fig. 3, we have

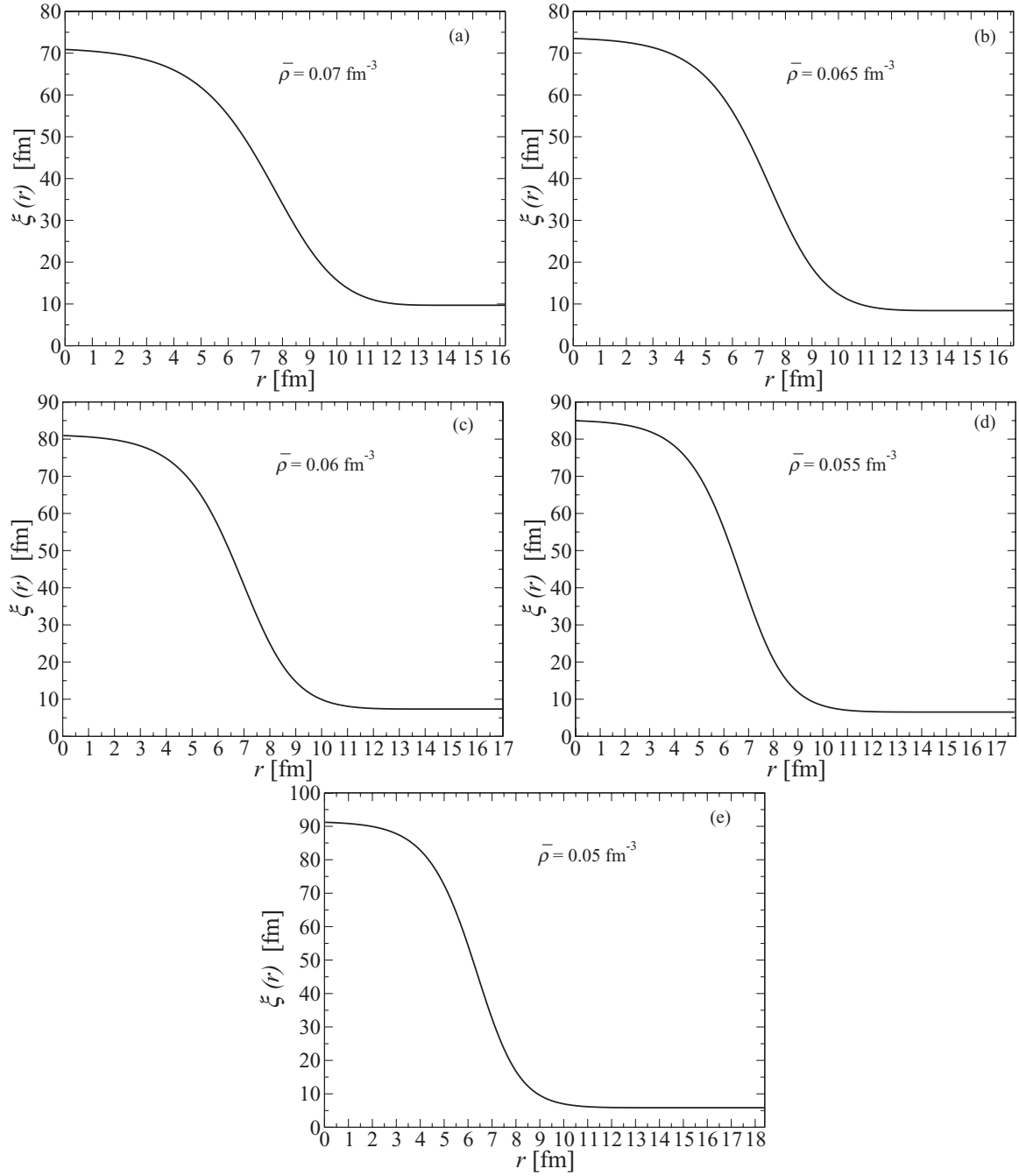

FIG. 5. Local coherence length, defined by Eq. (24), for the different crustal layers at $T = 0$.

found that they all share the same universal temperature dependence, which (for $^1S_0$ pairing) can be well represented by [41]

$$\Delta_{\alpha k}(T \leqslant T_c) \simeq \Delta_{\alpha k}(0)\sqrt{1-\left(\frac{T}{T_c}\right)^{\delta}}, \tag{26}$$

with $\delta \simeq 3.23$ and the critical temperature T_c, is defined by the condition $\Delta_{\alpha k}(T \geqslant T_c) = 0$ for all states. For simplicity, we have assumed that the composition remains unchanged at finite temperature so that the s.p. energies $\varepsilon_{\alpha k}$ and the matrix elements $V_{\alpha k \beta k'}$ are independent of T. We have determined T_c for each crustal layer by solving numerically Eqs. (3). For comparison, we have also calculated the critical temperature T_{cu} of a uniform neutron superfluid with the corresponding neutron background density ρ_{Bn}. As indicated in Table IV, the actual critical temperature T_c is systematically lower than T_{cu}, as could have been expected from the results on the pairing gaps discussed in Sec. V. The critical temperature $\bar{T}_{cu}$ of a uniform neutron superfluid with the average neutron density $\bar{\rho}_n$ is much closer to T_c.

It is well known from the BCS theory of superconductivity that the ratio of the critical temperature to the pairing gap is universal [2]. We have checked that this relation holds in

TABLE IV. Critical temperature for the onset of neutron superfluidity in the neutron-star crust for different average nucleon densities $\bar{\rho}$ using different approximations: T_c is the critical temperature obtained after solving the BCS Eqs. (3) numerically, while T_{cu} and $\bar{T}_{cu}$ are the critical temperatures of a uniform superfluid with density ρ_{Bn} and $\bar{\rho}_n$, respectively. All temperatures are indicated in units of 10^{10} K.

$\bar{\rho}$ (fm^{-3})	T_{cu}	T_c	$\bar{T}_{cu}$
0.070	1.17	0.96	0.94
0.065	1.31	1.09	1.08
0.060	1.45	1.24	1.23
0.055	1.58	1.38	1.38
0.050	1.70	1.52	1.53

uniform neutron matter, namely,

$$T_{cu} = \frac{\exp(\zeta)}{\pi}\Delta_u, \tag{27}$$

(likewise for $\bar{T}_{cu}$), where $\zeta \simeq 0.577$ is the Euler-Mascheroni constant. (This result is not specific to the pairing model we have used. It has also been found in microscopic calculations using realistic nucleon-nucleon interactions, as discussed in Ref. [42].) What is perhaps more surprising is that we have found the same relation for the inhomogeneous neutron superfluid in the neutron-star crust:

$$\frac{T_c}{\Delta_F} \simeq \frac{\exp(\zeta)}{\pi} \tag{28}$$

(note that in the original BCS theory [2], the superconductor is supposed to be isotropic and uniform). Because the band theory includes the limiting case in which all neutrons are bound inside clusters, we expect Eq. (28) to remain valid in finite nuclei. Quite interestingly, this conclusion seems to be supported by self-consistent mean-field calculations in tin isotopes [43], even though in this case the averaged gap Δ_F has to be suitably defined.

We can understand Eq. (28) by considering a simple pairing model. Because Eq. (28) holds in very different situations, this means that, unlike the state-dependent pairing gaps $\Delta_{\alpha k}$, the critical temperature is rather insensitive to the precise nature of s.p. states (see also Ref. [44] for a mathematical discussion in the context of multiband superconductivity). This suggests replacing the pairing matrix $V_{\alpha k \beta k'}$ with a constant coupling $\langle V\rangle/\mathcal{V}_{cell}$. In this case the pairing gaps $\Delta_{\alpha k}$ all become equal to the same value Δ and Eq. (3) reduces to the finite-temperature isotropic BCS gap equations,

$$1 = -\frac{1}{2}\frac{\langle V\rangle}{\mathcal{V}_{cell}}\int_0^{\mu+\varepsilon_\Lambda} d\varepsilon \frac{g(\varepsilon)}{E(\varepsilon)}\tanh\frac{E(\varepsilon)}{2T}, \tag{29}$$

where $E(\varepsilon) = \sqrt{(\varepsilon-\mu)^2+\Delta^2}$ is the q.p. energy, and $g(\varepsilon)$ is the density of s.p. states (for a given spin state), defined by

$$g(\varepsilon) = \sum_{\alpha,k}\delta(\varepsilon_{\alpha k} - \varepsilon). \tag{30}$$

The critical temperature T_c is mainly determined by unbound neutron s.p. states (see the discussion in Sec. V). However, as shown in a previous work [45], the density of unbound neutron s.p. states is essentially unaffected by the inhomogeneities on an energy scale larger than a few hundred keV. Because the pairing gaps are typically of the order of MeV, we can replace $g(\varepsilon)$ with its expression in uniform neutron matter with density $\bar{\rho}_n$,

$$g(\varepsilon) \simeq \frac{\mathcal{V}_{cell}}{4\pi^2}\left(\frac{2\bar{M}_n^*}{\hbar^2}\right)^{3/2}\sqrt{\varepsilon}, \tag{31}$$

where $\bar{M}_n^*$ is the corresponding neutron effective mass. At $T = 0$ the neutron chemical potential μ_n is given by the neutron Fermi energy,

$$\varepsilon_F = \frac{\hbar^2 k_F^2}{2\bar{M}_n^*}, \tag{32}$$

with $k_F = (3\pi^2\bar{\rho}_n)^{1/3}$. Because $T_c \ll \varepsilon_F$, we take $\mu(T_c) \simeq \varepsilon_F$, remembering that the lowest order correction is only of order $(T_c/\varepsilon_F)^2$. Because the most important contribution to the integral in Eq. (29) comes from s.p. states lying in the vicinity of the Fermi surface, we replace $g(\varepsilon)$ with $g(\varepsilon_F)$. For $T = T_c$, $\Delta = 0$, and Eq. (29) thus becomes

$$-\frac{4\pi^2\hbar^2}{\langle V\rangle\bar{M}_n^* k_F} = \int_{-\varepsilon_F/2T_c}^{\varepsilon_\Lambda/2T_c} dx \frac{\tanh|x|}{|x|}. \tag{33}$$

After remarking that $T_c \ll \varepsilon_\Lambda$, the integral in Eq. (33) can be solved analytically using

$$\int_0^y dx\frac{\tanh x}{x} \simeq \log\left(\frac{4y}{\pi}\right) + \zeta \tag{34}$$

for $y \gg 1$. Replacing Eq. (34) in Eq. (33), we find that the critical temperature is given by

$$T_c = \frac{2\exp(\zeta)}{\pi}\sqrt{\varepsilon_F\varepsilon_\Lambda}\exp\left(\frac{8\pi^2\hbar^2}{k_F\bar{M}_n^*\langle V\rangle}\right). \tag{35}$$

On the other hand, we assume that the average pairing gap Δ_F can be obtained from the solution of the BCS gap, Eq. (3), at $T = 0$ after substituting the pairing matrix $V_{\alpha k\beta k'}$ with the same pairing constant $\langle V\rangle/\mathcal{V}_{cell}$ that was introduced previously for calculating T_c. Equation (3) thus reduces to Eq. (29), which, at $T = 0$, reads

$$-\frac{4\pi^2\hbar^2}{\langle V\rangle\bar{M}_n^* k_F} = \int_{-\varepsilon_F/\Delta}^{\varepsilon_\Lambda/\Delta} dx(1+x^2)^{-1/2}, \tag{36}$$

where we have taken the density of states out of the integral. Solving Eq. (36) for the pairing gap yields

$$\Delta_F = \Delta = 2\sqrt{\varepsilon_F\varepsilon_\Lambda}\exp\left(\frac{8\pi^2\hbar^2}{k_F\bar{M}_n^*\langle V\rangle}\right). \tag{37}$$

Comparing Eqs. (35) and (37) leads to Eq. (28).

VII. FINITE-TEMPERATURE EFFECTS ON THE NEUTRON PAIRING FIELD

At finite temperatures, the pairing field is still given by the same expression (19) as for $T = 0$. But the normal neutron

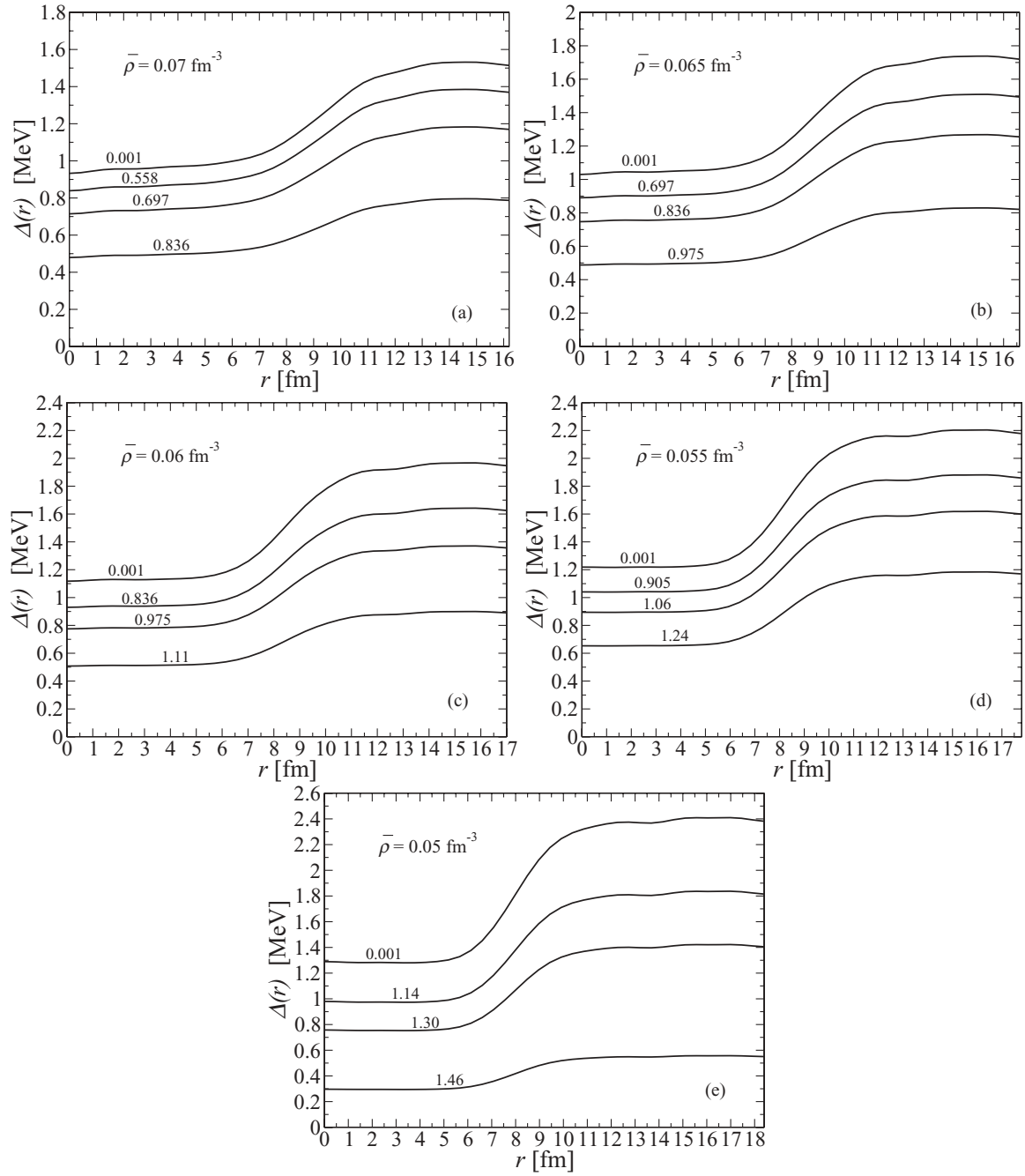

FIG. 6. Angle-averaged neutron pairing field $\Delta(r)$ for the different crustal layers at different temperatures. (T is indicated above each curve in 10^{10} K).

density and abnormal neutron density are now given by

$$\rho_n(\boldsymbol{r}) = \sum_{\alpha,\boldsymbol{k}}^{\Lambda} |\varphi_{\alpha\boldsymbol{k}}(\boldsymbol{r})|^2 \left[1 - \frac{\varepsilon_{\alpha\boldsymbol{k}} - \mu}{E_{\alpha\boldsymbol{k}}} \tanh \frac{E_{\alpha\boldsymbol{k}}}{2T}\right], \quad (38)$$

$$\tilde{\rho}_n(\boldsymbol{r}) = \sum_{\alpha,\boldsymbol{k}}^{\Lambda} |\varphi_{\alpha\boldsymbol{k}}(\boldsymbol{r})|^2 \frac{\Delta_{\alpha\boldsymbol{k}}}{E_{\alpha\boldsymbol{k}}} \tanh \frac{E_{\alpha\boldsymbol{k}}}{2T}. \quad (39)$$

In the LDA, the corresponding pairing field is given by

$$\Delta_n^{(\mathrm{LDA})}(\boldsymbol{r}, T) = \Delta_{\mathrm{u}}(\rho_n(\boldsymbol{r}))\sqrt{1 - \left(\frac{T}{T_{\mathrm{cu}}(\boldsymbol{r})}\right)^{\delta}} \quad (40)$$

for $T < T_{\mathrm{cu}}(\boldsymbol{r})$, with

$$T_{\mathrm{cu}}(\boldsymbol{r}) = \frac{\exp(\zeta)}{\pi} \Delta_{\mathrm{u}}(\rho_n(\boldsymbol{r})), \quad (41)$$

while for $T \geqslant T_{\mathrm{cu}}(\boldsymbol{r})$, $\Delta_n^{(\mathrm{LDA})}(\boldsymbol{r}, T) = 0$. Figure 6 shows the pairing field for different temperatures. The temperature dependence of the pairing field comes mainly from that of the abnormal density. As the temperature gets closer to the critical temperature T_{c}, the superfluid becomes more and more homogeneous. This is because the coherence length obtained after substituting $\Delta_n^{(\mathrm{LDA})}(\boldsymbol{r})$ with $\Delta_n^{(\mathrm{LDA})}(\boldsymbol{r}, T)$ in Eq. (24) increases with T and even diverges when the local

critical temperature is reached. This means that the LDA becomes worse at finite temperatures, strongly overestimating the impact of inhomogeneities. In particular, Eq. (40) implies that $\Delta_n^{(\mathrm{LDA})}(\boldsymbol{r}, T_{\mathrm{cu}}(0))$ vanishes inside clusters, while it remains finite outside, leading to a sharp variation of the pairing field at the cluster surface.

VIII. SPECIFIC HEAT OF SUPERFLUID NEUTRONS

Observations of the thermal X-ray emission from newly born isolated neutron stars can potentially provide valuable information on the structure of neutron-star crusts. Because of its relatively low neutrino emissivity, the crust of the neutron star cools less rapidly than the core and thus stays hotter. As a result, the surface temperature decreases slowly during the first ten to hundred years after the formation of the neutron star in a supernova explosion and then drops sharply when the cooling wave from the core reaches the surface [7,8]. The occurrence of neutron superfluidity in the inner crust has a strong influence on the neutron specific heat and, in turn, on the thermal relaxation time of the crust [9,10].

In Ref. [45], we have shown that the specific heat of normal neutrons in the outermost layers of the inner crust is almost unaffected by the nuclear lattice and is essentially given by the specific heat of a uniform gas. At low temperatures $T < T_{\mathrm{c}}$, pairing correlations have to be taken into account. This is usually done by introducing a multiplication factor $\mathcal{R}$, defined by

$$C_V^{(sn)} = \mathcal{R} C_V^{(n)}, \tag{42}$$

where $C_V^{(sn)}$ and $C_V^{(n)}$ are the specific heat of superfluid and normal neutrons, respectively. Assuming that the free neutrons are uniformly distributed, the factor $\mathcal{R}$ is well approximated by the analytical expression of Ref. [46] (used in neutron-star cooling simulations),

$$\mathcal{R}(y) = [0.4186 + \sqrt{1.007^2 + (0.501u)^2}] \times \exp(1.456 - \sqrt{1.456^2 + u^2}), \tag{43}$$

with $y = T/T_{\mathrm{cu}}$ and

$$u = \sqrt{1-y}\left(1.456 - \frac{0.157}{\sqrt{y}} + \frac{1.764}{y}\right). \tag{44}$$

To assess the validity of these expressions for the inhomogeneous matter of neutron-star crusts, we have evaluated the neutron specific heat from the numerical solutions of the anisotropic multiband BCS gap equations (3). We have applied the following expression from Ref. [47] using the temperature dependence of the gaps given by Eq. (26):

$$C_V^{(sn)} = \frac{1}{\mathcal{V}_{\mathrm{cell}}} \sum_{\alpha,k} \frac{\exp(E_{\alpha\boldsymbol{k}}/T)}{[1+\exp(E_{\alpha\boldsymbol{k}}/T)]^2} \times \left[\left(\frac{E_{\alpha\boldsymbol{k}}}{T}\right)^2 - \frac{1}{2T}\frac{\mathrm{d}}{\mathrm{d}T}\Delta_{\alpha\boldsymbol{k}}(T)^2\right]. \tag{45}$$

Numerical results are shown in Fig. 7. The summation in $\boldsymbol{k}$ space in Eq. (45) was carried out using the special-point method [37].

At low temperatures $T \ll T_{\mathrm{c}}$, neutron pairing correlations are very strong. The pairing gaps are weakly dependent on T and the last term in Eq. (45) is negligible (de Genne approximation [47]). In this regime, the neutron specific heat is exponentially suppressed compared to that of normal neutrons and decays approximately as $\exp(-\Delta_{\mathrm{F}}/T)$. However, as the temperature gets higher, the contribution of the last term in Eq. (45) becomes increasingly large, eventually leading to a sharp rise in the specific heat for $T \lesssim T_{\mathrm{c}}$. For $T > T_{\mathrm{c}}$, all pairing gaps vanish and neutron superfluidity is destroyed. For $T > T_{\mathrm{c}}$ and $T \ll \varepsilon_{\mathrm{F}}$, the specific heat increases linearly with T as clearly shown in Fig. 7. As in our previous work [45], we have found that the numerical results for the normal neutron specific heat are in good agreement with the expression for a uniform gas:

$$C_V^{(n)} = \frac{\bar{M}_n^* k_{\mathrm{F}}}{3\hbar^2} T. \tag{46}$$

Note, however, that for the dense crustal layers considered here, using $\bar{M}_n^*$ and k_{F} instead of M_{Bn}^* and $k_{\mathrm{F}B}$ (as in Ref. [45]) yields a slightly better fit. As shown in Fig. 7, the transition between the superfluid and the normal regime is very sharp. The specific heat exhibits a discontinuity at $T = T_{\mathrm{c}}$, approximately given by

$$\frac{C_V^{(sn)}(T_{\mathrm{c}}) - C_V^{(n)}(T_{\mathrm{c}})}{C_V^{(n)}(T_{\mathrm{c}})} \simeq \frac{3}{2}\delta \exp(-2\zeta), \tag{47}$$

after replacing $\Delta_{\alpha\boldsymbol{k}}$ with Δ_{F} in Eq. (45) and the density of the s.p. state by Eq. (31). Note that for $T \lesssim T_{\mathrm{c}}$, the neutron specific heat is enhanced by pairing, that is, $\mathcal{R} > 1$.

We have found that $C_V^{(sn)}$ is numerically close to the expression for a uniform superfluid, namely, Eqs. (42), (43), and (46), *provided* that the critical temperature is suitably renormalized (i.e., T_{cu} must be replaced with T_{c}) as shown in Fig. 7 (renormalized homogeneous superfluid curve).

IX. CONCLUSIONS

We have clarified the effects of the nuclear inhomogeneities on the neutron superfluidity in the deep layers of the neutron-star crust by solving the anisotropic multiband BCS gap equations (3). We have properly taken into account the interactions between the neutron superfluid and the nuclear crystal lattice by imposing Bloch boundary conditions instead of using the W-S approximation. Because of the presence of the nuclear clusters, neutrons belonging to different bands and having different Bloch wave vectors undergo different pairing interactions, thus leading to a dispersion of the neutron pairing gaps $\Delta_{\alpha\boldsymbol{k}}$ of about 0.2–0.4 MeV around the Fermi level, as shown in Fig. 3. The neutron pairing gap Δ_{F} *averaged* over all continuum states is reduced owing to the presence of inhomogeneities, but much less than predicted by previous calculations based on the W-S approximation [27]. Unlike the individual gaps $\Delta_{\alpha\boldsymbol{k}}$, Δ_{F} is essentially unaffected by the band structure and is very well approximated by the gap $\bar{\Delta}_{\mathrm{u}}$ in uniform neutron matter using the average neutron density $\bar{\rho}_n$. The reason for this agreement lies in the highly nonlocal

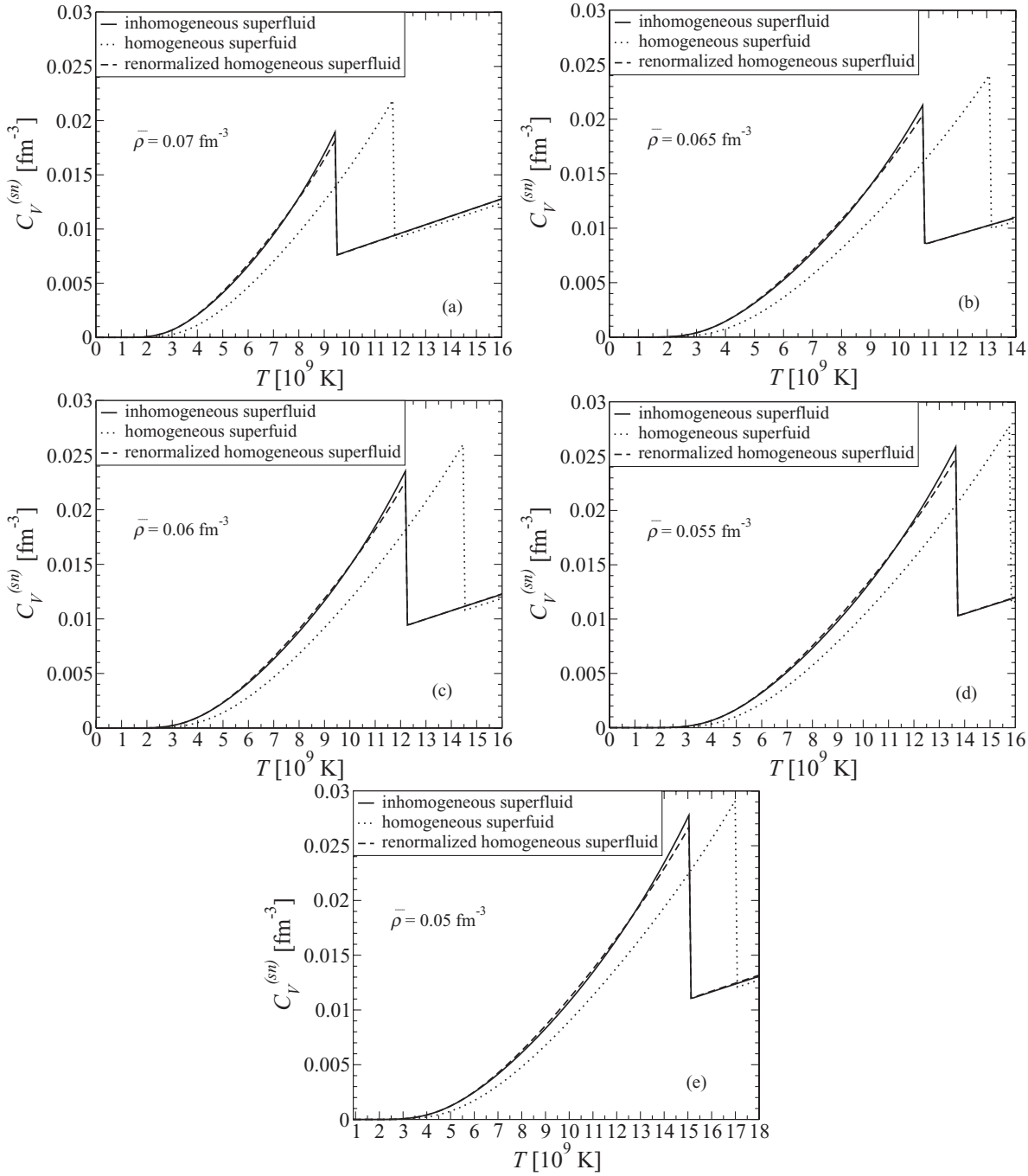

FIG. 7. Specific heat of superfluid neutrons in different layers of the inner crust of a neutron star. The solid line has been obtained from Eq. (45) after solving numerically the BCS Eqs. (3) The dashed and dotted lines correspond to homogeneous neutron matter with two different values of the critical temperature T_c and T_{cu}, respectively.

character of the pairing phenomenon involving both bound and unbound neutrons, as revealed by numerical calculations of the neutron pairing field $\Delta_n(\boldsymbol{r})$. As a consequence, the LDA strongly overestimates the spatial variations of the pairing field. The discrepancies are particularly large inside clusters, where the LDA incorrectly predicts a quenching of pairing correlations.

Solving the BCS equations at finite temperatures, we have found that the temperature dependence of the pairing gaps $\Delta_{\alpha \boldsymbol{k}}$ is universal and well represented by Eq. (26). Unlike what one may have naively expected, the critical temperature T_c is not determined by the largest state-dependent pairing gap around the Fermi level but, rather, by the average pairing gap Δ_F. Moreover, the ratio T_c/Δ_F is approximately given by the BCS value $\simeq 0.58$ [2]. We have explained these results by solving the isotropic BCS Eqs. (29) in the weak-coupling approximation, leading to the analytical expression (35) for the critical temperature. We have computed

the neutron pairing field at finite temperatures and we have shown that the LDA becomes worse as the temperature is increased.

We have computed the neutron specific heat, which is an important ingredient for modeling the thermal evolution of newly born neutron stars [7–10]. We have found that the specific heat is modified by clusters but it can be easily estimated from the expression in uniform neutron matter, namely, Eqs. (42), (43), and (46), by simply renormalizing T_c.

The conclusions of the present work may change in shallower regions of the crust where the matter is more inhomogeneous, as suggested by a recent study in dirty superconductors [48]. In addition, we have neglected the change in composition with increasing temperature [34], which could affect the values of the pairing gaps (hence also the critical temperature) for $T \gtrsim 10^{10}$ K. In particular, we expect to find deviations of the ratio T_c/Δ_F from the BCS value of $\simeq 0.58$ when these thermal effects are taken into account. We have also left aside the modifications of the pairing gaps owing to many-body effects beyond the BCS approximation [49]. These various issues will be addressed in future work using the multiband approach presented in this paper.

ACKNOWLEDGMENTS

N.C. acknowledges financial support from a Marie Curie Intra-European Grant (Contract No. MEIF-CT-2005-024660). This work was also supported by FNRS (Belgium), by NSERC (Canada), and by CompStar, a Research Networking Programme of the European Science Foundation.

[1] A. B. Migdal, Nucl. Phys. **13**, 655 (1959).
[2] J. Bardeen, L. N. Cooper, and J. R. Schrieffer, Phys. Rev. **108**, 1175 (1957).
[3] G. Baym, C. J. Pethick, and D. Pines, Nature **224**, 673 (1969).
[4] P. W. Anderson and N. Itoh, Nature **256**, 25 (1975).
[5] N. Chamel and B. Carter, Mon. Not. R. Astron. Soc. **368**, 796 (2006).
[6] K. Glampedakis and N. Andersson, Phys. Rev. Lett. **102**, 141101 (2009).
[7] J. M. Lattimer, K. A. van Riper, M. Prakash, and M. Prakash, Astrophys. J. **425**, 802 (1994).
[8] O. Y. Gnedin, D. G. Yakovlev, and A. Y. Potekhin, Mon. Not. R. Astron. Soc. **324**, 725 (2001).
[9] C. Monrozeau, J. Margueron, and N. Sandulescu, Phys. Rev. C **75**, 065807 (2007).
[10] M. Fortin, F. Grill, J. Margueron, and N. Sandulescu, arXiv:0910.5488.
[11] D. N. Aguilera, V. Cirigliano, J. A. Pons, S. Reddy, and R. Sharma, Phys. Rev. Lett. **102**, 091101 (2009).
[12] P. S. Shternin, D. G. Yakovlev, P. Haensel, and A. Y. Potekhin, Mon. Not. R. Astron. Soc. Lett. **382**, L43 (2007).
[13] E. F. Brown and A. Cumming, Astrophys. J. **698**, 1020 (2009).
[14] B. Carter, N. Chamel, and P. Haensel, Nucl. Phys. A **748**, 675 (2005).
[15] N. Chamel, Nucl. Phys. A **747**, 109 (2005).
[16] L. Samuelsson and N. Andersson, Class. Quant. Grav. **26**, 155016 (2009).
[17] D. J. Dean and M. Hjorth-Jensen, Rev. Mod. Phys. **75**, 607 (2003).
[18] F. V. De Blasio, M. Hjorth-Jensen, Ø. Elgarøy, L. Engvik, G. Lazzari, M. Baldo, and H.-J. Schulze, Phys. Rev. C **56**, 2332 (1997).
[19] M. Matsuo, Phys. Rev. C **73**, 044309 (2006).
[20] N. Chamel and P. Haensel, Living Rev. Relativ. **11**, 10 (2008); http://www.livingreviews.org/lrr-2008-10.
[21] M. Tinkham, *Introduction to Superconductivity* (McGraw–Hill, New York, 1996).
[22] F. Barranco, R. A. Broglia, H. Esbensen, and E. Vigezzi, Phys. Lett. B **390**, 13 (1997).
[23] F. Barranco, R. A. Broglia, H. Esbensen, and E. Vigezzi, Phys. Rev. C **58**, 1257 (1998).
[24] F. Montani, C. May, and H. Müther, Phys. Rev. C **69**, 065801 (2004).
[25] N. Sandulescu, N. Van Giai, and R. J. Liotta, Phys. Rev. C **69**, 045802 (2004); N. Sandulescu, *ibid.* **70**, 025801 (2004).
[26] E. Khan, N. Sandulescu, and N. Van Giai, Phys. Rev. C **71**, 042801(R) (2005).
[27] M. Baldo, E. E. Saperstein, and S. V. Tolokonnikov, Eur. Phys. J. A **32**, 97 (2007).
[28] M. Baldo, E. E. Saperstein, and S. V. Tolokonnikov, Nucl. Phys. A **775**, 235 (2006).
[29] N. Chamel, S. Naimi, E. Khan, and J. Margueron, Phys. Rev. C **75**, 055806 (2007).
[30] H. Suhl, B. T. Matthias, and L. R. Walker, Phys. Rev. Lett. **3**, 552 (1959).
[31] H. J. Choi, D. Roundy, H. Sun, M. L. Cohen, and S. G. Louie, Nature **418**, 758 (2002).
[32] M. Iavarone *et al.*, Phys. Rev. Lett. **89**, 187002 (2002).
[33] F. Hunte, J. Jaroszynski, A. Gurevich, D. C. Larbalestier, R. Jin, A. S. Sefat, M. A. McGuire, B. C. Sales, D. K. Christen, and D. Mandrus, Nature **453**, 903 (2008).
[34] M. Onsi, A. K. Dutta, H. Chatri, S. Goriely, N. Chamel, and J. M. Pearson, Phys. Rev. C **77**, 065805 (2008).
[35] K. Oyamatsu and M. Yamada, Nucl. Phys. A **578**, 181 (1994).
[36] N. Chamel, S. Goriely, and J. M. Pearson, Nucl. Phys. A **812**, 72 (2008).
[37] J. Hama and M. Watanabe, J. Phys. Condens. Matter **4**, 4583 (1992).
[38] A. Baldereschi, Phys. Rev. B **7**, 5212 (1973).
[39] A. Baldereschi and E. Tosatti, Phys. Rev. B **17**, 4710 (1978).
[40] E. A. Rakhmanov, E. B. Saff, and Y. M. Zhou, Math. Res. Lett. **1**, 647 (1994).
[41] S. Goriely, Nucl. Phys. A **605**, 28 (1996).
[42] U. Lombardo, in *Nuclear Methods and Nuclear Equation of State*, edited by M. Baldo (World Scientific, Singapore, 1999), pp. 458–510.

[43] E. Khan, N. Van Giai, and N. Sandulescu, Nucl. Phys. A **789**, 94 (2007).
[44] Y. Yang, Physica D **200**, 60 (2005).
[45] N. Chamel, J. Margueron, and E. Khan, Phys. Rev. C **79**, 012801(R) (2009).
[46] K. P. Levenfish and D. G. Yakovlev, Astron. Rep. **38**, 247 (1994).
[47] P. G. de Gennes, *Superconductivity of Metals and Alloys* (W. A. Benjamin, New York, 1966), p. 129.
[48] Y. Zou, I. Klich, and G. Refael, Phys. Rev. B **77**, 144523 (2008).
[49] E. Vigezzi, F. Barranco, R. A. Broglia, G. Colò, G. Gori, and F. Ramponi, Nucl. Phys. A **752**, 600 (2005).